Catalytic efficiencies for methane removal: Impact of HOx, NOx and chemistry in the high-chlorine regime

Luisa Pennacchio,[†,§] Maarten van Herpen,[‡,§] Daphne Meidan,[¶] Alfonso Saiz-Lopez,[¶] and Matthew S. Johnson[*,†]

†*Department of Chemistry, University of Copenhagen, Universitetsparken 5, DK-2100 Copenhagen, Denmark.*

‡*Acacia Impact Innovation BV, Acacialaan 9, 5384 BB, Heesch, The Netherlands.*

¶*Department of Atmospheric Chemistry and Climate, Institute of Physical Chemistry Blas Cabrera, CSIC, Madrid 28006, Spain.*

§*These authors contributed equally to this work.*

E-mail: msj@chem.ku.dk

Abstract

Catalytic production of chlorine atoms from iron salt aerosols has been suggested as a means of achieving atmospheric methane removal. The feasibility of this approach, its efficiency and the optimum conditions for deployment must be determined, but this is not straightforward as the mechanism involves interlocking nonlinear atmospheric free radical chain reactions; under some conditions added chlorine is known to increase methane lifetime. Here we evaluate the catalytic efficiency of atmospheric methane oxidation under different conditions, initiated by the photocatalytic conversion of chloride to chlorine by iron chlorides Fe(III)$\mathrm{Cl}_n^{(3-n)}$ using a box model. While HOx and

high NOx behaviors are well known, a new regime for tropospheric chemistry is found and described, one characterized by high ClOx conditions. We find that at chlorine production rates below 1×10^6 Cl_2 /(cm^3 s) and ambient NOx and O_3 levels of 4–80 ppt NOx at 14 ppb O_3, 8–180 ppt NOx at 30 ppb O_3 and 14–200 ppt NOx at 40 ppb O_3 the net effect on CH_4 is negative, increasing CH_4 concentrations. This variation is driven by the formation and hydrolysis of $ClONO_2$ leading to loss of O_3 and NO_2. At high rates of Cl_2 addition the reaction of CH_3OOH with Cl becomes the major source of OH and CH_4 is removed. At elevated ClOx, $ClO^{\cdot}$ usurps the role of NO in converting HO_2 to OH, and CH_3O_2 to CH_3O. The efficiencies seen in the model range from -0.62 to 2.81 CH_4/Cl. The modeling shows that due to the dispersion of a ship's plume into low NOx conditions, iron emitted by ships is likely to increase the lifetime of atmospheric methane.

Introduction

Methane is a potent greenhouse gas, responsible for >1/3 of global warming since pre-industrial times;[1] its atmospheric burden continues to increase with a new record set every year for over a decade.[2] The IPCC emissions pathways that prevent 1.5 °C of global warming by 2050 require large reductions of methane emissions.[1] The obvious strategy would be to reduce emissions from the largest methane sources including agriculture, fossil fuels, and waste and wastewater. However, according to Höglund-Isaksson *et al.*, emissions reduction is limited to 30-45% by 2030 and 50% by 2050 using known technologies. Moreover, emissions from natural sources including wetlands, permafrost, thermokarst lakes and bacterial processes are likely to increase with increasing global temperature.[4–6] Wetland emissions could increase by 22 to 149% by 2100, becoming larger than anthropogenic emissions in most scenarios.[7] Already, about half of the increased methane concentration in 2020 can be attributed to wetland emissions.[6]

Due to the challenge of reducing atmospheric methane in the face of increasing anthro-

pogenic and natural emissions, it may be necessary to develop method/s to remove methane from the atmosphere, similar to carbon dioxide removal.[8–10] According to recent work, atmospheric methane removal has the potential to reduce global average temperature by 0.4-1 °C.[11–13] The IPCC concluded that the field is in its infancy.[1]

Photocatalytic generation of chlorine by iron salt aerosols (ISA) has been suggested as a method for achieving cost-effective atmospheric methane removal.[14,15] The method has been demonstrated in the laboratory.[16–19] In addition to the low technology readiness level there are important questions regarding the safety, efficacy, appropriate conditions for, and especially the governance of any such approach.[20] It was recently shown that the ISA mechanism is active over the North Atlantic in Mineral Dust-Sea Spray Aerosols (MDSA) created when particles from the Sahara descend into the marine boundary layer (MBL).[21] Unexpectedly, MDSA is the largest source of oxidized chlorine (Cl_2 and Cl) in this region. The largest anthropogenic source of iron in the MBL is shipping, arising from impurities in fuel. This source was estimated at <16 Gg(Fe)/yr in 2001.[22] These anthropogenic emissions of soluble iron will likely mix with sea-salt aerosols, creating ISA that would produce chlorine, possibly removing methane.[14,23] Herrmann and coauthors have summarized research on the photochemistry of aqueous iron complexes including a wide variety of inorganic and organic ligands.[24] Additionally, Hoffmann and coauthors constructed a detailed model of marine multiphase chemistry for air quality in polluted coastal areas.[25] In particular, the simulations indicate significant influence of Cl atoms on the oxidation of volatile organic compounds.

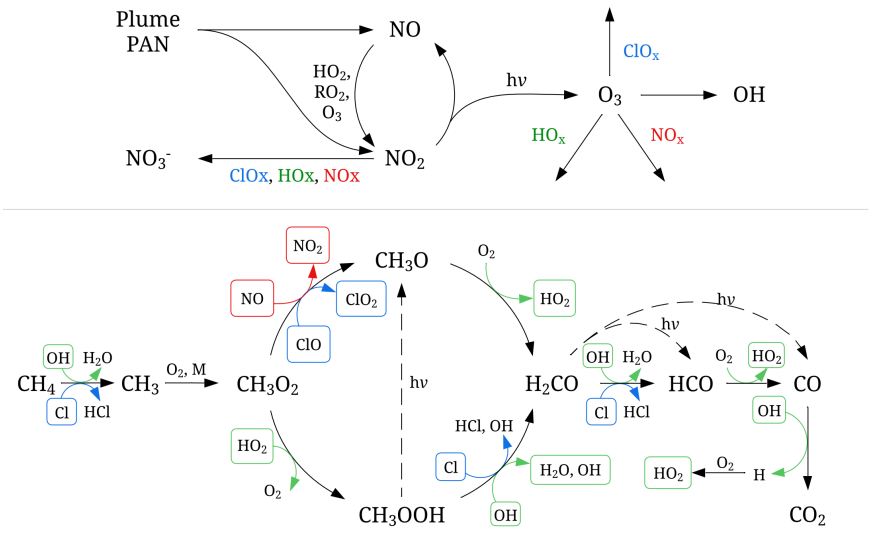

Figure 1: Schematic showing the interlocking atmospheric radical cycles. Top, overview of the HOx, NOx and ClOx cycles' interactions and their effect on O_3 concentrations. Bottom, methane oxidation mechanism, including HOx (green), NOx (red) and ClOx (blue) species.

Previous research has shown that while $Cl^{\cdot}$ can be important in initiating oxidation of methane and non-methane volatile organic compounds,[26] a higher rate of $Cl^{\cdot}$ production does not necessarily lead to a reduction in methane as the additional $Cl^{\cdot}$ can suppress methane removal by $OH^{\cdot}$.[21,27,28] This is because $OH^{\cdot}$ production depends on O_3 and NO_2, both of which are removed by ClOx, see Figure 1, top. However, the negative impact of lower $OH^{\cdot}$ concentrations on methane removal can be overcome with sufficiently high rate of Cl_2 addition.[28] It is important to consider these effects when evaluating the impact of iron from shipping on methane, especially as NOx plays an important role in the mechanism and ships co-emit NOx with iron.

In this paper, we use a photochemical box model to evaluate the impact of adding Cl_2 to the troposphere on methane removal for a wide range of parameters extending from a concentrated nascent shipping exhaust plume to the ambient atmosphere. We assess the impact as methane removal per added Cl_2 at different atmospheric NOx levels.

Method

A box model that runs a diurnal cycle and constant NOx input was built in the Kintecus environment.[29] The model contains the radical cycles and the oxidation of CH_4 and dimethyl sulfide (DMS), as it impacts NOx at night.[30] The mechanisms and rates of these reactions were obtained from the Master Chemical Mechanism, MCM v3.3.1,[31–33] via website: www.mcm.york.ac.uk. The model uses a reduced VOC chemistry but contains the key elements to describe the system, specifically the interlocking free radical chain reactions, see Figure 1, top. The model includes the ClOx reactions and key deposition rates. Furthermore, bromine and iodine chemistry was included due to their importance in the MBL.[34–37]

A full listing of the initial conditions and the reactions and their sources can be found in the Supporting Information (SI). Photolysis reactions not included in the MCM subscheme are obtained from the NCAR TUV calculator.[38] NOx and O_3 are constrained via fixed emissions of NO_2 and $O(^3P)$ rather than fixed concentrations.[39] This allows for the evaluation of the impact of the radical chemistry on methane. Constraining O_3 gives more realistic levels due to the mixing of the atmosphere. Thus, an additional first order loss rate of O_3 is added at high NOx as well.

The model is run for 16 days to reach stable concentrations for key species like O_3 and NOx. Next, Cl_2 is added ('A' for 1 day at a maximum rate r_{A,Cl_2} depending linearly on solar intensity $I(t)$. The model is run for 15 additional days to let it relax to baseline concentrations. CH_4 oxidation initiated by $OH^{\cdot}$ and $Cl^{\cdot}$ is tracked during the 16-day period after Cl_2 release starts and compared with the same model run with no addition of chlorine, i.e. r_{A,Cl_2}=0. CH_4 removal is divided by total Cl emission $n_{T,Cl}$ to derive CH_4 removal per Cl. The total emission is given by:

$$n_{T,\mathrm{Cl}} = 2 \int r_{A,\mathrm{Cl}_2}\, I(t) dt \ , \ I(t) \in [0,1] \tag{1}$$

The addition of Cl_2 affects methane oxidation by $OH^{\cdot}$ in three ways: ClOx removes 1)

NO_2 and 2) O_3 reducing $OH^{\cdot}$ production, see Figure 1, top, and 3) $ClOx$ affects the HOx radical chain efficiency.

The model output was benchmarked against the Community Earth System Model (CESM) by Meidan *et al.* by converting Cl_2 emission rates to daily average Cl_2 mixing ratios, see SI. The CESM output for the North Pacific (NP) and North Atlantic (NA) regional boxes were used.

Ozone production efficiency, ϵ_{O_3}

The ozone production efficiency, ϵ_{O_3}, is defined as the rate of O_3 production ('P') (r_{P,O_3}) divided by the rate of NOx loss ('L') ($r_{L,NOx}$): $\epsilon_{O_3} = r_{P,O_3}/r_{L,NOx}$.[41] The photolysis of NO_2 will produce O_3, however, NO_2 is also lost to oxidation to nitrate $r = k[NO_2][OH^{\cdot}][M]$, see Figure 1, top. The balance between the rate of photolysis and the rate of HNO_3 formation determines ϵ_{O_3}. This number depends on local conditions and is mainly driven by solar intensity, temperature and $[OH^{\cdot}]$.

Values of ϵ_{O_3} over the United States are typically in the range 1-20. In the remote troposphere, where NOx levels are very low, ϵ_{O_3} is much higher and can even exceed 100.[41]

O_3-$OH^{\cdot}$ production efficiency, β_{O_3}

The O_3-$OH^{\cdot}$ production efficiency, β_{O_3}, is defined as the total rate of O_3 loss divided by the production rate of OH at midday: $\beta_{O_3} = r^{Tot}_{L,O3}/r^{Noon}_{P,OH}$. $OH^{\cdot}$ is produced through the photolysis of O_3 followed by reaction with water:

$$O_3 + h\nu \rightarrow O_2 + O(^1D) \quad \text{(R1)}$$

$$O(^1D) + M \rightarrow O(^3P) + M \quad \text{(R2)}$$

$$O(^3P) + O_2 + M \rightarrow O_3 + M \quad \text{(R3)}$$

$$O(^1D) + H_2O \rightarrow 2\,OH^{\cdot} \quad \text{(R4)}$$

Reaction (R1) does not always lead to loss of O_3 due to reactions (R2) and (R3). O_3 is lost in (R4) to yield two $OH^{\cdot}$ radicals. Other loss reactions for O_3 include reactions with HOx and NOx as well as deposition:

$$O_3 + HO_2 \rightarrow OH^{\cdot} + 2\,O_2 \quad \text{(R5)}$$

$$O_3 + OH^{\cdot} \rightarrow HO_2 + O_2 \quad \text{(R6)}$$

$$O_3 + NO \rightarrow O_2 + NO_2 \quad \text{(R7)}$$

$$O_3 + NO_2 \rightarrow O_2 + NO_3 \quad \text{(R8)}$$

while photolysis of NO_2 from (R7) produces O_3 via (R3), closing a null cycle, the competing formation of HNO_3 should be included in loss rate of O_3, r_{L,O_3}. Addition of $Cl^{\cdot}$ creates an additional loss for O_3 through (R9), reducing β_{O_3}.

$$Cl + O_3 \rightarrow ClO + O_2 \quad \text{(R9)}$$

Radical chain length, ν_{OH}

Methane is oxidized in a nonlinear chain reaction where $OH^{\cdot}$ is both reagent and product, see Figure 1, bottom. Due to these feedbacks, an additional $OH^{\cdot}$ can ultimately cause more than one $OH^{\cdot}$ reaction.[42] This amplification is described by the radical chain length, defined as the rate of loss of $OH^{\cdot}$ divided by the rate of $OH^{\cdot}$ primary production via (R1)-(R4): $\nu_{OH} = \frac{r_{L,OH}}{r_{PP,OH}}$. At steady state $r_{L,OH} = r_{P,OH}$ where $r_{P,OH}$ is the rate of production of $OH^{\cdot}$ by all processes.

In high-NOx conditions the CH_4 oxidation chain reaction produces one NO_2 and three HO_2 radicals, which together produce four $OH^{\cdot}$ through reactions (R3),(R10) and (R11),

replacing $OH^{\cdot}$ lost to reaction and producing additional ozone, increasing $OH^{\cdot}$:[43]

$$HO_2 + NO \rightarrow OH^{\cdot} + NO_2 \quad \text{(R10)}$$

$$NO_2 + h\nu \rightarrow NO + O \quad \text{(R11)}$$

followed by (R3). In low-NOx conditions the mechanism only produces one HO_2. Without (R10) HO_2 increases, forming H_2O_2 and terminating the chain. The radical chain length is thus much shorter under low-NOx conditions making the efficiency of CH_4 removal by $OH^{\cdot}$ much lower.

Results and Discussion

The model yields stable concentrations over the full time-period and the results are reproducible. The modeled $OH^{\cdot}$ concentration over the entire NOx range, $[OH^{\cdot}] = 6.5 \times 10^6$ to 2.2×10^7 cm^{-3}, is slightly higher than the literature, 7×10^5 to 2.9×10^6 cm^{-3}, which can be attributed to the limited VOC chemistry in the box model.[44–46] In comparable conditions, there is good agreement with Edwards and Young, see SI. The box model and the CESM[40] output show similar NOx and O_3 depletion with increasing Cl_2 emissions. Additionally, $ClONO_2$ is also in good agreement, with slightly higher concentrations in CESM, suggesting the hydrolysis rate used in our box model is in the same order of magnitude as the NP and NA locations in CESM. Furthermore, H_2O_2 concentrations increase similarly in both models, as well as HOCl and CH_3OOH which are indicative of the high-ClOx regime, see SI S8. The agreement between CESM and the box model provides high confidence in the conclusions based on the box model investigation.

Sensitivity analyses are performed for the $ClONO_2$ hydrolysis rate, due to the variability in the aerosol surface area in the MBL, and for the effect of additional ozone sources and sinks. The effect of iodine and bromine chemistry is discussed in SI, and was found to only

have a minor impact.

Ozone production efficiency, ϵ_{O_3}

In the model, NOx is mainly lost through reaction with OH$^{\cdot}$ giving HNO_3. The large addition of Cl$^{\cdot}$ introduces another loss mechanism for NO_2 via formation of $ClONO_2$ which can either be photolyzed back to ClO$^{\cdot}$ and NO_2 or hydrolyze forming HNO_3:

$$ClO + NO_2 + M \rightarrow ClONO_2 + M \quad \text{(R12)}$$

$$ClONO_2 + H_2O_{(l)} \rightarrow HNO_3 + HOCl \quad \text{(R13)}$$

$H_2O_{(l)}$ is high in the MBL so (R13) is very fast with a rate limited by the diffusion of $ClONO_2$ to a particle. The HOCl formed in (R13) can be photolyzed to OH$^{\cdot}$ and Cl$^{\cdot}$ or absorbed by particles, where it can react either with HCl/Cl^- to form Cl_2 [18,35] or be deposited with the particle.

Increased chlorine addition increases the rate of NOx loss $r_{L,\mathrm{NOx}}$, decreasing the ozone production efficiency ϵ_{O_3}. Figure S1 shows the ozone production efficiency as a function of x_{NOx} and r_{A,Cl_2} (peak rate at noon). Very large addition of Cl_2 reduces ϵ_{O_3} by an order of magnitude, from >100 to the range of 10 to 30.

The NOx lost under high Cl$^{\cdot}$ conditions reduces O_3 production. While the reduction of tropospheric O_3 and NOx pollution is desirable for health and the environment, it results in lower OH$^{\cdot}$ production from O_3 via (R1) and (R4).

O_3-OH$^{\cdot}$ production efficiency, β_{O_3}

The O_3-OH$^{\cdot}$ production efficiency, β_{O_3}, as a function of the NOx mixing ratio x_{NOx} and r_{A,Cl_2} is shown in Figure S2. β_{O_3} is highest at low NOx and low-Cl_2 conditions, with a maximum of 0.84 mol OH$^{\cdot}$/mol O_3. Under these conditions the photolysis of O_3 followed by reaction with H_2O to form OH$^{\cdot}$ is the main O_3 sink, see Figure S3 which illustrates the O_3 sinks at

low and high NOx. The lowest β_{O_3} values are found for high-NOx and high-Cl_2 conditions which suppress O_3, preventing $OH^{\cdot}$ formation. β_{O_3} increases above $r_{A,Cl_2} \approx 10^6$ Cl_2 /(cm^3 s) as $Cl^{\cdot}$ reacts with NO, decreasing this loss of O_3. Above this range most O_3 is lost by (R9), decreasing $r_{P,OH}$, but increasing the radical chain length, described in the next section.

Radical chain length, ν_{OH}

The main $OH^{\cdot}$ sink reactions at high and low NOx are shown in the top of Figure 2 as a function of r_{A,Cl_2}. $OH^{\cdot}$ loss increases sharply with increasing Cl_2 addition in low NOx/high ClOx conditions. This does not necessarily mean that [$OH^{\cdot}$] will decrease as the radical chain length ν_{OH} could increase due to increased $OH^{\cdot}$ production by other mechanisms.

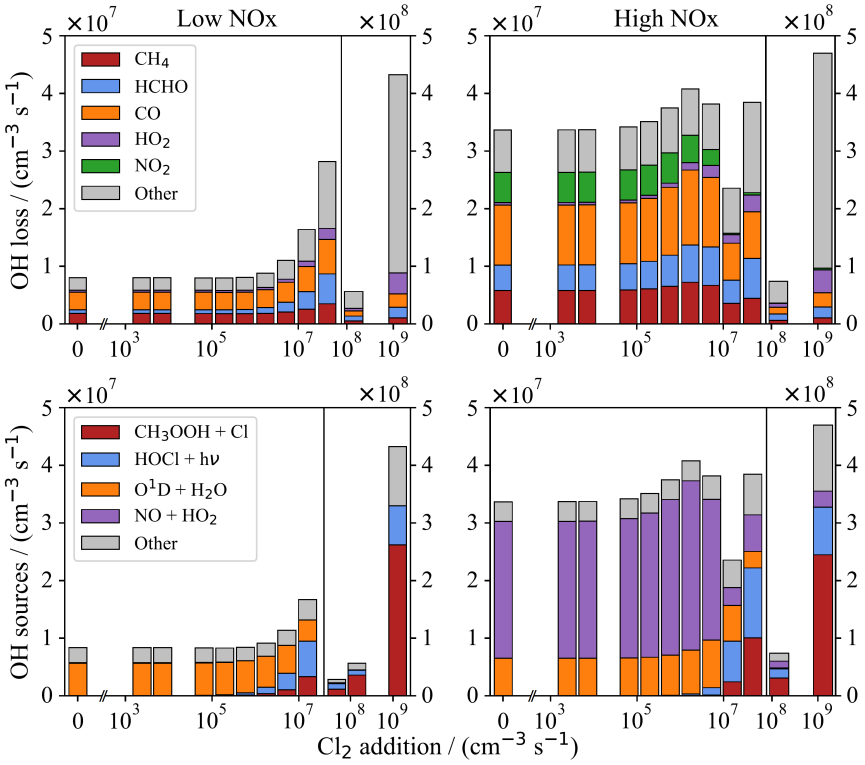

Figure 2: Overview of the main $OH^{\cdot}$ reactions ($r_{L,OH}$, top) and sources ($r_{P,OH}$, bottom) at peak sunlight with increasing r_{A,Cl_2} at low NOx (9 ppt) (left) and high NOx (4 pbb) (right). Note the different y-axes.

The main sources of $OH^{\cdot}$ for low- and high-NOx conditions, with increasing r_{A,Cl_2}, are shown at the bottom of Figure 2. $OH^{\cdot}$ from O_3 ($O(^1D)+H_2O$) is suppressed at high r_{A,Cl_2}

due to (R9). However, alternative $OH^{\cdot}$ sources at high r_{A,Cl_2} become dominant, increasing ν_{OH}. In low-NOx conditions reaction (R14) becomes the main $OH^{\cdot}$ source above 10^6 Cl_2 /(cm^3 s) while at high NOx the photolysis of HOCl becomes the dominant source of $OH^{\cdot}$ as r_{A,Cl_2} increases, followed by (R14) at the very highest r_{A,Cl_2}.

$$Cl^{\cdot} + CH_3OOH \rightarrow HCl + CH_2O + OH^{\cdot} \quad \text{(R14)}$$

The $OH^{\cdot}$ chain length at peak sunlight as a function of x_{NOx} and r_{A,Cl_2} is shown in Figure S4. As expected ν_{OH} is shorter in low-NOx conditions, <2, as methane oxidation is forced through the HOx pathway, see Figure 2. For high-NOx conditions ν_{OH} increases to 2.2-5.2. Above 1×10^7 Cl_2 /(cm^3 s) there is a dramatic increase in ν_{OH}, due to additional $OH^{\cdot}$ sources from $Cl^{\cdot}$ chemistry, see Figure 2 bottom.

Although the formation of $ClO^{\cdot}$ in (R9) decreases $OH^{\cdot}$ by consuming O_3, $ClO^{\cdot}$ can reform O_3 and $ClO^{\cdot}$ can make the methane oxidation cycle more efficient. An overview of the interactions is shown in Figure S5. At low-NOx, the $ClO^{\cdot}$ reaction with CH_3O_2 (R15) is substantial, providing an alternative to the low NOx pathway, see Figure 1, bottom. Moreover, a substantial fraction of $ClO^{\cdot}$ reacts with HO_2, (R16), converting it into $OH^{\cdot}$ through the formation and photolysis of HOCl.

$$ClO + CH_3O_2 \rightarrow Cl^{\cdot} + HCHO + HO_2 \quad \text{(R15)}$$

$$ClO + HO_2 \rightarrow HOCl + O_2 \quad \text{(R16)}$$

At high NOx conditions $ClO^{\cdot}$ mainly reacts with NO and NO_2, depleting NOx, which can lead to low NOx conditions. The reaction of $ClO^{\cdot}$ with NO produces NO_2 which can be photolyzed, reforming the O_3 used to make $ClO^{\cdot}$. Even at low-NOx conditions this reaction will occur and represents 10% of the total loss of $ClO^{\cdot}$ for r_{A,Cl_2} below 4×10^4 Cl_2 /(cm^3 s).

CH_4 removal

The overall efficiency of the mechanism depends on the three parameters introduced above: the O_3 production efficiency ϵ_{O3}, the O_3-$OH^{\cdot}$ production efficiency β_{O_3} and the radical chain length ν_{OH}. The combined impact is seen by calculating the change in $[CH_4]$ per emitted Cl atom over the simulation period, see Figure 3. The effect of added Cl_2 depends strongly on x_{NOx} and r_{A,Cl_2}. At $x_{NOx} < 4$ ppt (4×10^{-12} mol/mol) or > 180 ppt (1.8×10^{-10} mol/mol) the effect is always positive, removing additional CH_4. Between these x_{NOx} levels and below 1×10^6 Cl_2 /(cm^3 s), $\Delta[CH_4]$ is negative, i.e. $[CH_4]$ increases. This range is dependent on the $ClONO_2$ hydrolysis rate, see below. The most favorable regime is for $x_{NOx} > 1$ ppb (1×10^{-9} mol/mol), where as many as 2.81 CH_4 can be removed per Cl. Comparing with the CESM output from Meidan *et al.*, the same unfavorable NOx range can be observed, but extends up to 1×10^7 Cl_2 /(cm^3 s). Differences between the CESM and the box model could be due to the wide fluctuation of NOx/O_3 and Cl_2 emission in CESM, or due to the added VOC chemistry included in CESM.

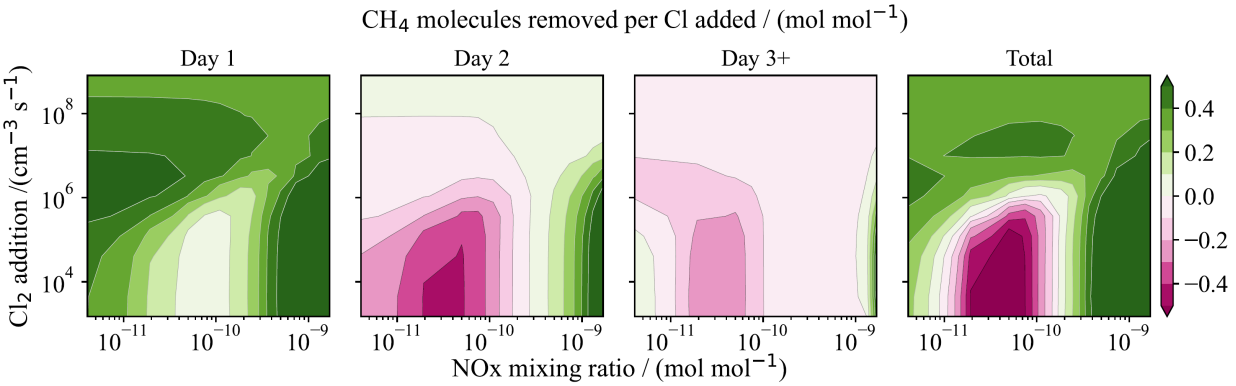

Figure 3: CH_4 removed per added Cl (mol/mol) as a function of x_{NOx} and maximum r_{A,Cl_2}, split over the days when the impact is observed and a total time of 16 days. The darkest pink ranges from -0.62 to -0.4 and the darkest green ranges from 0.5 to 2.81

While changes to ν_{OH} occur during emission, the impacts of O_3 loss continue for at least a day and the impact of NOx loss continues for several days. This is seen in the CH_4 removal per day shown in Figure 3. On the day of Cl_2 emission CH_4 removal, increases in

all scenarios. However, on day 2 the impact of O_3 loss leads to an increase in $[CH_4]$ in all scenarios except high NOx and high r_{A,Cl_2}. For days 3-16, overall, the loss of NOx leads to lower O_3 formation and lower $OH^{\cdot}$ production, resulting in increased $[CH_4]$ for all conditions except high NOx with low r_{A,Cl_2} and very low NOx. Thus, the impact of r_{A,Cl_2} cannot be judged just based on measurements on the day of emission, but needs to take several days after emission into account.

Sensitivity Analyses

$ClONO_2$ hydrolysis rate sensitivity analysis

Reaction of $ClO^{\cdot}$ with NO_2 will produce $ClONO_2$ which can hydrolyze yielding HOCl and HNO_3. The HNO_3 will most likely be deposited and thereby the reaction represents the main loss of NOx due to Cl_2 addition. The hydrolysis rate of $ClONO_2$, however, is dependent on particle surface area density, which changes over orders of magnitude. The rate has been approximated as a first order reaction and the sensitivity of the model was tested by evaluating CH_4 removal per Cl atom added, when the total emission is 1500 Cl_2 molecules/(cm^3 s), see Figure S6. Deiber *et al.* reported a $ClONO_2$ uptake coefficient of 0.02 on water and NaCl solution. Using a thermal velocity of 277 m/s and a sea spray aerosol surface area density in the range of 1 – 50 $\mu m^2/cm^3$ (depending on wind speed)[48] results in a first order loss rate for $ClONO_2$ hydrolysis ranging from 5.5×10^{-6} s^{-1} to 2.8×10^{-4} s^{-1}, and hydrolysis rates may be further increased due to mineral dust or emitted iron salt aerosols. Therefore, we used an average value of 10^{-4} s^{-1} in our model (corresponding to 20 $\mu m^2/cm^3$ surface area density), and we performed a sensitivity analysis covering the range of 10^{-3} s^{-1} to 10^{-6} s^{-1}.

The hydrolysis rate competes with the photolysis rates of 10^{-5} s^{-1}, producing Cl and NO_3, and 10^{-6} s^{-1}, producing $ClO^{\cdot}$ and NO_2 again. A fast hydrolysis rate will therefore result in a higher NOx removal, which in turn will decrease the O_3 production and the following OH production. Ultimately, this will lead to increasing CH_4 concentrations when the NOx

mixing ratio is between 4–200 ppt (4×10^{-12}–2×10^{-10} mol/mol) with a hydrolysis rate of 10^{-3} s^{-1}. This is in agreement with the findings reported by Edwards and Young.[39] In contrast, decreasing the hydrolysis rate to 10^{-5} s^{-1} will result in CH_4 removal at all NOx mixing ratios.

Sensitivity to additional ozone sources and sinks

The reduction of ozone due to the addition of chlorine atoms to the atmosphere is highly relevant for our conclusions. We performed a sensitivity analysis using an extra source of ozone and an extra sink of ozone in the box model, see Figure 4. A sensitivity analysis was performed without constraining O_3 with additional sources or sinks, which resulted in relatively low O_3 at low NOx, and relatively high O_3 at high NOx, and the resulting methane removal per Cl was in line with the simulations where O_3 was constrained. The sensitivity analysis shows that increasing O_3 leads to less CH_4 removal in high-NOx conditions and more removal in low-NOx conditions. Increasing [CH_4] is found between 4–80 ppt NOx at 14 ppb O_3, 8–180 ppt NOx at 30 ppb O_3 and 14–200 ppt NOx at 40 ppb O_3.

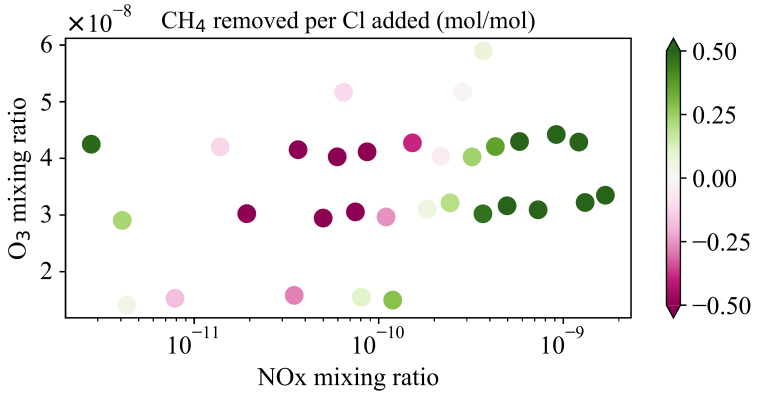

Figure 4: O_3 sensitivity analysis evaluating CH_4 removed per Cl added as a function of NOx and O_3 mixing ratios, with r_{A,Cl_2} =1500 $Cl_2/(cm^3\ s)$.

Relevance for ship emissions

Iron present in fuel or additives is emitted as part of a ship's plume. As the plume disperses, iron containing particles will mix with sea spray aerosols, forming ISA. These aerosols could

potentially produce high intensity Cl_2 emissions within the high NOx conditions of the plume. However, ship plumes disperse rapidly, reducing the concentration of the ISA and NOx by orders of magnitude, while spreading the aerosols over a very large area. Typically, the dispersion into the background will occur within a day, but the ISA could have a total atmospheric lifetime of several days, depending on particle size.[49] This implies that the impact of the shipping iron emission is driven by the local, ambient NOx concentrations where the plume disperses.

Based on Figure 3 it can be seen that low r_{A,Cl_2} leads to an increase in $[CH_4]$ for x_{NOx} from 4-180 ppt, while Figure 4 shows that this range is shifted higher with increasing $[O_3]$. This results in increased $[CH_4]$ between 4–80 ppt NOx at 14 ppb O_3, 8–180 ppt NOx at 30 ppb O_3 and 14–200 ppt NOx at 40 ppb O_3. Figure 5 shows the areas where these conditions occur in red, based on the yearly average from the CESM global model output for 2023. The model description can be found in Meidan *et al.*. Most of the world has unfavorable background NOx and O_3 concentrations, which means that shipping iron emissions are likely to increase methane levels. One exception is a region in the North Atlantic, which explains why mineral dust in this region was able to effectively remove methane from the atmosphere, as shown by van Herpen *et al.*. A constant rate of 10^{-4} s^{-1} for the $ClONO_2$ hydrolysis has been used for this analysis. However, the local aerosol surface area density is dependent on wind speed, resulting in faster and slower hydrolysis rates regionally. As discussed above, this will have an impact on the methane removal.

Conclusion

In this paper we have explored a new domain of tropospheric chemistry, the high ClOx regime. The results of the study show clearly that the impact of chlorine added to the atmosphere depends critically on ambient conditions. Initial chlorine can increase methane lifetime via its effects on ozone and NOx, the primary and secondary sources of the main

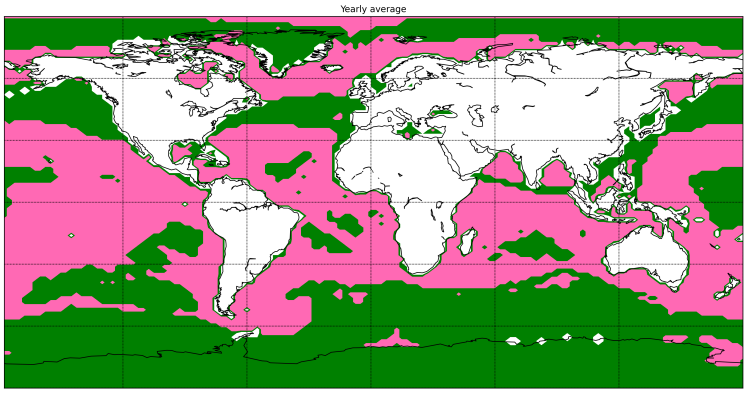

Figure 5: World map highlighting the unfavorable NOx and O_3 levels, 4–80 ppt NOx at 14 ppb O_3, 8–180 ppt NOx at 30 ppb O_3 and 14–200 ppt NOx at 40 ppb O_3, for low r_{A,Cl_2} where CH_4 concentration increase in pink, using the yearly average NOx and O_3 surface concentrations from the CESM global model output for 2023. NOx and O_3 levels resulting in net CH_4 removal is indicated by green. Model description can be found in Meidan *et al.*.

methane oxidant, $OH^{\cdot}$. The impact of chlorine depends on the amount of NOx present. We have identified the range of NOx and O_3 concentrations, 4–80 ppt NOx at 14 ppb O_3, 8–180 ppt NOx at 30 ppb O_3 and 14–200 ppt NOx at 40 ppb O_3, where Cl_2 emissions below $1{\times}10^6$ /(cm^3 s) lead to an increase of CH_4 lifetime. Cl_2 emissions above this threshold always lead to net CH_4 removal. At such high Cl_2 additions $CH_3OOH + Cl^{\cdot}$ becomes the dominant $OH^{\cdot}$ source. In addition, in the high-ClOx regime, $ClO^{\cdot}$ reacts with CH_3O_2 and HO_2 resulting in Cl and increasing OH radical chain length. The impact of Cl_2 emissions should not just be evaluated on the day of emission, as it has a longer term impact through the loss of O_3 and NOx. This is especially important to keep in mind for atmospheric measurements. We identified the main reaction responsible for the ozone and associated OH loss, which is $ClO^{\cdot} + NO_2 \rightarrow ClONO_2$, followed by hydrolysis of $ClONO_2$. Without $ClONO_2$ hydrolysis, ozone loss is strongly reduced and methane lifetime does not increase. However, the hydrolysis rate in the troposphere is variable, due to changing particle surface area density and uncertainty regarding the hydrolysis rate itself, as few studies exist. More research is needed to reduce these uncertainties.

Ship plume emissions dilute quickly, making ISA particles from ship emissions spend most of their lifetime in the range of low-Cl_2 emissions and local background levels of NOx.

This implies that the impact of ISA from shipping strongly depends on the NOx and O_3 concentrations in the area the ship plume is dispersed into. We show that due to this effect, for most of the world, ship based ISA emissions can lead to an increase of methane. Iron emissions from ships are likely to increase methane lifetime, while removing ozone and NOx pollution.

These findings are important to the discussion of how much chlorine would be required to reduce methane and restore it to preindustrial concentrations.[28] It is also important as chlorine sources do not release chlorine equally in terms of surface flux or volumetric rate, as assumed e.g. by Li *et al.*. The proposed methods of introducing iron to the atmosphere are point sources,[14,15,28] resulting in a high-ClOx regime that cannot be captured with global models due to dilution to grid dimensions.[49] However, we have shown that the impact of Cl_2 emissions needs to be evaluated over multiple days. Because of the long term effects on O_3 and NOx loss the impact cannot be captured easily with a local box model as dilution will depend on meteorology. Therefore, both local plume modeling and global modeling need to be combined to fully appreciate the effects of Cl_2 from iron emissions by ships.

Acknowledgement

The authors are grateful for support from Spark Climate Solutions and the ISAMO project.

The University of Copenhagen (UCPH) has filed a patent application related to atmospheric iron chlorides on behalf of its inventors (MvH, MSJ). All other authors declare they have no competing interests.

Supporting Information Available

The following Supporting Information is available free of charge at the ACS website:

Figure S1. Ozone production efficiency.

Figure S2. O_3-OH production efficiency.

Figure S3. O_3 sinks.

Figure S4. $OH^{\cdot}$ chain length, ν_{OH}.

Figure S5. $ClOx$ chemistry and $ClO^{\cdot}$ sinks.

Figure S6. CH_4 removal comparison with CESM.

Figure S7. Comparison with CESM.

Figure S8. $ClONO_2$ hydrolysis rate sensitivity.

Model evaluation and sensitivity analyses.

Model setup and full list of reactions.

References

(1) IPCC In *Climate Change 2021: The Physical Science Basis. Contribution of Working Group I to the Sixth Assessment Report of the Intergovernmental Panel on Climate Change*; Masson-Delmotte, V. *et al.* , Eds.; Cambridge University Press: Cambridge, United Kingdom and New York, NY, USA, 2021; pp 3–32.

(2) Lan, X.; Thoning, K.; Dlugokencky, E. Trends in globally-averaged CH4 N2O, and SF6 determined from NOAA Global Monitoring Laboratory measurements, Version 2023-04, NOAA Earth System Research Laboratories Global Monitoring Laboratory. 2023.

(3) Höglund-Isaksson, L.; Gómez-Sanabria, A.; Klimont, Z.; Rafaj, P.; Schöpp, W. Technical potentials and costs for reducing global anthropogenic methane emissions in the 2050 timeframe –results from the GAINS model. *Environmental Research Communications* **2020**, *2*, 025004.

(4) Neumann, R. B.; Moorberg, C. J.; Lundquist, J. D.; Turner, J. C.; Waldrop, M. P.; McFarland, J. W.; Euskirchen, E. S.; Edgar, C. W.; Turetsky, M. R. Warming effects

of spring rainfall increase methane emissions from thawing permafrost. *Geophysical Research Letters* **2019**, *46*, 1393–1401.

(5) Paudel, R.; Mahowald, N. M.; Hess, P. G.; Meng, L.; Riley, W. J. Attribution of changes in global wetland methane emissions from pre-industrial to present using CLM4. 5-BGC. *Environmental Research Letters* **2016**, *11*, 034020.

(6) Peng, S.; Lin, X.; Thompson, R. L.; Xi, Y.; Liu, G.; Hauglustaine, D.; Lan, X.; Poulter, B.; Ramonet, M.; Saunois, M.; others Wetland emission and atmospheric sink changes explain methane growth in 2020. *Nature* **2022**, *612*, 477–482.

(7) Kleinen, T.; Gromov, S.; Steil, B.; Brovkin, V. Atmospheric methane underestimated in future climate projections. *Environmental Research Letters* **2021**, *16*, 094006.

(8) Jackson, R. B.; Abernethy, S.; Canadell, J. G.; Cargnello, M.; Davis, S. J.; Féron, S.; Fuss, S.; Heyer, A. J.; Hong, C.; Jones, C. D.; others Atmospheric methane removal: a research agenda. *Philosophical Transactions of the Royal Society A* **2021**, *379*, 20200454.

(9) Nisbet-Jones, P. B.; Fernandez, J. M.; Fisher, R. E.; France, J. L.; Lowry, D.; Waltham, D. A.; Woolley Maisch, C. A.; Nisbet, E. G. Is the destruction or removal of atmospheric methane a worthwhile option? *Philosophical Transactions of the Royal Society A* **2022**, *380*, 20210108.

(10) Pennacchio, L.; Mikkelsen, M. K.; Krogsbøll, M.; van Herpen, M. M. J. W.; Johnson, M. Physical and practical constraints on atmospheric methane removal technologies. *Environmental Research Letters* **2024**,

(11) Smith, C.; Mathison, C. How much methane removal is required to avoid overshooting 1.5°C? *Environmental Research Letters* **2024**, *19*, 074044.

(12) Abernethy, S.; O'Connor, F. M.; Jones, C. D.; Jackson, R. B. Methane removal and the proportional reductions in surface temperature and ozone. *Philosophical Transactions of the Royal Society A: Mathematical, Physical and Engineering Sciences* **2021**, *379*, 20210104.

(13) Staniaszek, Z.; Griffiths, P. T.; Folberth, G. A.; O'Connor, F. M.; Archibald, A. T. Climate and composition impacts of a net-zero anthropogenic methane future using an emissions-driven chemistry-climate model. EGU General Assembly Conference Abstracts. 2021; pp EGU21–5740.

(14) Oeste, F. D.; de Richter, R.; Ming, T.; Caillol, S. Climate engineering by mimicking natural dust climate control: the iron salt aerosol method. *Earth System Dynamics* **2017**, *8*, 1–54.

(15) Meyer-Oeste, F. D. Troposphere cooling procedure. 2014-07-09.

(16) Wittmer, J.; Bleicher, S.; Zetzsch, C. Iron(III)-Induced Activation of Chloride and Bromide from Modeled Salt Pans. *The Journal of Physical Chemistry A* **2015**, *119*, 4373–4385, PMID: 25243918.

(17) Wittmer, J.; Bleicher, S.; Ofner, J.; Zetzsch, C. Iron (III)-induced activation of chloride from artificial sea-salt aerosol. *Environmental Chemistry* **2015**, *12*, 461–475.

(18) Wittmer, J.; Zetzsch, C. Photochemical activation of chlorine by iron-oxide aerosol. *Journal of Atmospheric Chemistry* **2017**, *74*, 187–204.

(19) Mikkelsen, M. K.; Liisberg, J. B.; van Herpen, M. M. J. W.; Mikkelsen, K. V.; Johnson, M. S. Photocatalytic chloride to chlorine conversion by ionic iron in aqueous aerosols: A combined experimental, quantum chemical and chemical equilibrium model study. *Aerosol Research* **2023**, *ar-2023-13*, x.

(20) Gorham, K. A.; Abernethy, S.; Jones, T. R.; Hess, P.; Mahowald, N.; Meidan, D.; Johnson, M. S.; van Herpen, M. M. J. W.; Xu, Y.; Saiz-Lopez, A.; Röckmann, T.; Brashear, C.; Reinhardt, E.; Mann, D. An atmospheric methane removal roadmap: iron salt aerosols to enhance chlorine radicals. *Environmental Research Letters* **2023**, *xx*, xx–xx.

(21) van Herpen, M. M. J. W.; Li, Q.; Saiz-Lopez, A.; Liisberg, J. B.; Röckmann, T.; Cuevas, C. A.; Fernandez, R. P.; Mak, J. E.; Mahowald, N. M.; Hess, P.; Meidan, D.; Stuut, J.-B. W.; Johnson, M. S. Photocatalytic chlorine atom production on mineral dust–sea spray aerosols over the North Atlantic. *Proceedings of the National Academy of Sciences of the USA* **2023**, *XX*, XX.

(22) Ito, A. Global modeling study of potentially bioavailable iron input from shipboard aerosol sources to the ocean. *Global Biogeochemical Cycles* **2013**, *27*, 1–10.

(23) Ming, T.; de Richter, R.; Dietrich Oeste, F.; Tulip, R.; Caillol, S. A nature-based negative emissions technology able to remove atmospheric methane and other greenhouse gases. *Atmospheric Pollution Research* **2021**, *12*, 101035.

(24) Herrmann, H.; Schaefer, T.; Tilgner, A.; Styler, S. A.; Weller, C.; Teich, M.; Otto, T. Tropospheric aqueous-phase chemistry: kinetics, mechanisms, and its coupling to a changing gas phase. *Chemical reviews* **2015**, *115*, 4259–4334.

(25) Hoffmann, E. H.; Tilgner, A.; Vogelsberg, U.; Wolke, R.; Herrmann, H. Near-explicit multiphase modeling of halogen chemistry in a mixed urban and maritime coastal area. *ACS Earth and Space Chemistry* **2019**, *3*, 2452–2471.

(26) Young, C.; Washenfelder, R.; Edwards, P.; Parrish, D.; Gilman, J.; Kuster, W.; Mielke, L.; Osthoff, H.; Tsai, C.; Pikelnaya, O.; others Chlorine as a primary radical: evaluation of methods to understand its role in initiation of oxidative cycles. *Atmospheric chemistry and physics* **2014**, *14*, 3427–3440.

(27) Li, Q.; Fernandez, R. P.; Hossaini, R.; Iglesias-Suarez, F.; Cuevas, C. A.; Apel, E. C.; Kinnison, D. E.; Lamarque, J.-F.; Saiz-Lopez, A. Reactive halogens increase the global methane lifetime and radiative forcing in the 21st century. *Nature Communications* **2022**, *13*, 2768.

(28) Li, Q.; Meidan, D.; Hess, P.; Añel, J. A.; Cuevas, C. A.; Doney, S.; Fernandez, R. P.; van Herpen, M.; Höglund-Isaksson, L.; Johnson, M. S.; others Global environmental implications of atmospheric methane removal through chlorine-mediated chemistry-climate interactions. *Nature Communications* **2023**, *14*, 4045.

(29) Ianni, J. C. Kintecus, Windows Version 6.01. `http://www.kintecus.com`, 2017.

(30) Kim, H. S.; Kim, Y. H.; Song, C. H. Ship-plume sulfur chemistry: ITCT 2K2 case study. *Science of The Total Environment* **2013**, *450-451*, 178–187.

(31) Jenkin, M. E.; Saunders, S. M.; Pilling, M. J. The tropospheric degradation of volatile organic compounds: a protocol for mechanism development. *Atmospheric Environment* **1997**, *31*, 81–104.

(32) Saunders, S. M.; Jenkin, M. E.; Derwent, R. G.; Pilling, M. J. Protocol for the development of the Master Chemical Mechanism, MCM v3 (Part A): tropospheric degradation of non-aromatic volatile organic compounds. *Atmospheric Chemistry and Physics* **2003**, *3*, 161–180.

(33) Master Chemical Mechanism, MCM v3.2. `http://mcm.leeds.ac.uk/MCM`, 2023.

(34) Saiz-Lopez, A.; Shillito, J. A.; Coe, H.; Plane, J. M. C. Measurements and modelling of I_2, IO, OIO, BrO and NO_3 in the mid-latitude marine boundary layer. *Atmospheric Chemistry and Physics* **2006**, *6*, 1513–1528.

(35) Hossaini, R.; Chipperfield, M. P.; Saiz-Lopez, A.; Fernandez, R.; Monks, S.; Feng, W.; Brauer, P.; Von Glasow, R. A global model of tropospheric chlorine chemistry: Organic

versus inorganic sources and impact on methane oxidation. *Journal of Geophysical Research: Atmospheres* **2016**, *121*, 14–271.

(36) Saiz-Lopez, A.; Plane, J. M. C.; Mahajan, A. S.; Anderson, P. S.; Bauguitte, S. J.-B.; Jones, A. E.; Roscoe, H. K.; Salmon, R. A.; Bloss, W. J.; Lee, J. D.; Heard, D. E. On the vertical distribution of boundary layer halogens over coastal Antarctica: implications for O_3, HO_x, NO_x and the Hg lifetime. *Atmospheric Chemistry and Physics* **2008**, *8*, 887–900.

(37) Sander, S.; Friedl, R.; Golden, D.; Kurylo, M.; Moortgat, G.; Wine, P.; Ravishankara, A.; Kolb, C.; Molina, M.; Finlayson-Pitts, B.; others *Chemical kinetics and photochemical data for use in atmospheric studies evaluation number 15*; 2006.

(38) Madronich, S.; Flocke, S.; Zeng, J.; Petropavlovskikh, I.; Lee-Taylor, J. Tropospheric ultraviolet and visible (TUV) radiation model. 2002; National Center for Atmospheric Research (NCAR), Boulder, CO.

(39) Edwards, P. M.; Young, C. J. Primary Radical Effectiveness: Do the Different Chemical Reactivities of Hydroxyl and Chlorine Radicals Matter for Tropospheric Oxidation? *ACS ES&T Air* **0**, *0*, 546–554.

(40) Meidan, D.; Li, Q.; Cuevas, C. A.; Doney, S. C.; Fernandez, R. P.; van Herpen, M. M. J. W.; Johnson, M. S.; Kinnison, D. E.; Li, L.; Hamilton, D. S.; Saiz-Lopez, A.; Hess, P.; Mahowald, N. M. Evaluating the potential of iron-based interventions in methane reduction and climate mitigation. *Environmental Research Letters* **2024**, *19*, 054023.

(41) Jacob, D. J. *Introduction to Atmospheric Chemistry*; Princeton University Press: Princeton, 2000; pp 231–244.

(42) Levy, H. Normal atmosphere: Large radical and formaldehyde concentrations predicted. *Science* **1971**, *173*, 141–143.

(43) Harnung, S. E.; Johnson, M. S. *Chemistry and the Environment*; Cambridge University Press, 2012.

(44) Thompson, A.; Johnson, J.; Torres, A.; Bates, T.; Kelly, K.; Atlas, E.; Greenberg, J.; Donahue, N.; Yvon, S.; Saltzman, E.; others Ozone observations and a model of marine boundary layer photochemistry during SAGA 3. *Journal of Geophysical Research: Atmospheres* **1993**, *98*, 16955–16968.

(45) Cooper, D. J. Estimation of hydroxyl radical concentrations in the marine atmospheric boundary layer using a reactive atmospheric tracer. *Journal of atmospheric chemistry* **1996**, *25*, 97–113.

(46) Yang, M.; Blomquist, B. W.; Huebert, B. J. Constraining the concentration of the hydroxyl radical in a stratocumulus-topped marine boundary layer from sea-to-air eddy covariance flux measurements of dimethylsulfide. *Atmospheric Chemistry and Physics* **2009**, *9*, 9225–9236.

(47) Deiber, G.; George, C.; Le Calvé, S.; Schweitzer, F.; Mirabel, P. Uptake study of $ClONO_2$ and $BrONO_2$ by Halide containing droplets. *Atmospheric Chemistry and Physics* **2004**, *4*, 1291–1299.

(48) Moore, K. A.; Alexander, S. P.; Humphries, R. S.; Jensen, J.; Protat, A.; Reeves, J. M.; Sanchez, K. J.; Kreidenweis, S. M.; DeMott, P. J. Estimation of Sea Spray Aerosol Surface Area Over the Southern Ocean Using Scattering Measurements. *Journal of Geophysical Research: Atmospheres* **2022**, *127*, e2022JD037009, e2022JD037009 2022JD037009.

(49) Song, C. H.; Chen, G.; Hanna, S. R.; Crawford, J.; Davis, D. D. Dispersion and chemical evolution of ship plumes in the marine boundary layer: Investigation of O3/NOy/HOx chemistry. *Journal of Geophysical Research: Atmospheres* **2003**, *108*.